A new waveform inversion workflow: Application to near-surface velocity estimation in Saudi Arabia

Xukai Shen, Thierry Tonellot, Yi Luo, Tim Keho and Robert Ley

ABSTRACT

Waveform inversion is a more accurate near-surface velocity estimation tool than ray-based methods. It is able to solve complex near-surface velocity structure where conventional ray-based methods fail. If errors in the initial model are too large, waveform inversion will fail to converge to the correct model. This convergence problem is particularly obvious for large near-surface velocity contrasts and velocity inversions. We propose to address this issue with a new inversion workflow that adds a wave-equation traveltime inversion step prior to waveform inversion. The performance of our approach is evaluated on both synthetic and field data.

INTRODUCTION

Typically, conventional ray-based methods (Hampson and Russell, 1984; Olson, 1984; White, 1989) are used to derive near-surface velocity. Such smooth solutions may be adequate for areas with simple near-surface velocity distributions, but in geologically complex areas, smooth velocities are not accurate enough for imaging deeper reflectors (Marsden, 1993; Bevc, 1995; Hindriks and Verschuur, 2001). In such cases, waveform inversion (Tarantola, 1984; Pratt et al., 1998; Mora, 1987) tends to give more accurate results (Ravaut et al., 2004; Sheng et al., 2006; Sirgue et al., 2009) by simulating seismic wave propagation.

With more and more long offset data being acquired, particularly on land, it is not uncommon to see shingling in data (Figure 1). Shingling is defined here as where first-break traveltimes are only piecewise continuous when we look at data in shot gathers. This phenomenon is likely to be caused by a near-surface low velocity layer (Figure 2). Shingling poses a serious problem for ray-based inversion methods. Note that at the shot gather in Figure 1, the first-break amplitudes decay so much that that at a certain offset, the only reliable pick on a trace becomes the later refraction arrival in time. The discontinuity is caused by tracking different events as we move further away from source location. Since ray-based methods assume the same event is being picked, they tend to fail in these types of situations.

Waveform inversion relies on the wave equation and is able to solve the velocity structure quite well even in the presence of low velocity layers. Results from waveform

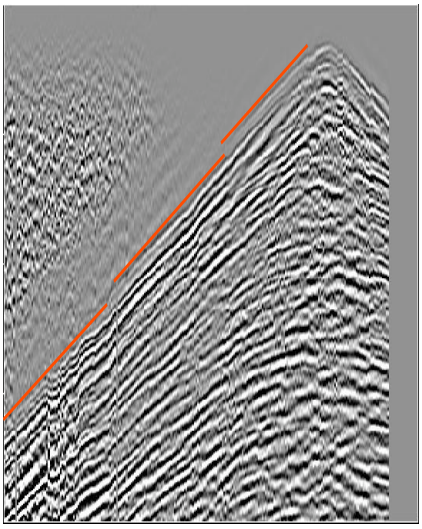

Figure 1: Shot gather of 2D land dataset showing shingling phenomenon, red lines denote approximate first-break picks, notice how they become discontinuous as offset increases.[**NR**]

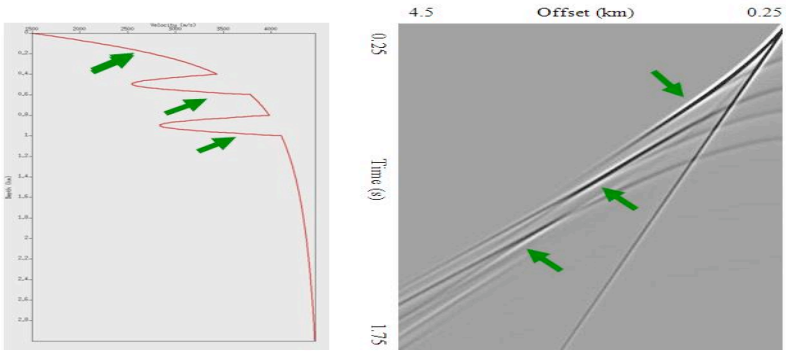

Figure 2: A synthetic data case showing a) a 1D velocity model with low velocity layers in the near-surface and b) the resulting shot gather. Green arrows denote decaying refractions on the right and where they occur in near-surface model on the left. [**NR**]

inversion are highly dependent on the accuracy of the starting model and on the frequency content of the data. To relax the dependence of the waveform inversion on the initial model, we propose the work flow described in the next section.

WAVEFORM INVERSION WORKFLOW

Our waveform inversion workflow consists of three successive steps:

```
1) First arrival traveltime tomography.
2) Wave-equation traveltime inversion.
3) Early arrival acoustic waveform inversion.
```

The first step relies on ray theory to estimate an initial low frequency velocity model to explain the first arrival picks. In the second step, we use the output of the conventional traveltime tomography as input to wave-equation traveltime inversion (Luo and Schuster, 1991). This result is then used as input for the third step of full waveform inversion. Since both the traveltime and waveform inversion are derived from the same wave-equation, they can both be described in a common framework where the objective function can be written as

$$f\left(\mathbf{d_{obs}}, \mathbf{D}(\mathbf{m})\right) \approx \mathbf{0}, \tag{1}$$

where f is a function of $\mathbf{d_{obs}}$ and $\mathbf{D}(\mathbf{m})$, the observed data and forward modeled synthetic data from the velocity model $\mathbf{m}$ respectively. Observed data can be either in frequency domain or in time domain, depending on the actual form of $\mathbf{f}$. For example if we take $\mathbf{f}$ as the L2 norm of $(\mathbf{d_{obs}} - \mathbf{D}(\mathbf{m}))$, we obtain the objective function of conventional waveform inversion (Tarantola, 1984; Pratt et al., 1998); if we take $\mathbf{f}$ as the L2 norm of the time lag difference of the cross-correlation of $\mathbf{D}(\mathbf{m})$ and $\mathbf{d_{obs}}$, we obtain an objective function for wave-equation traveltime inversion. (Luo and Schuster, 1991). This second formulation is more robust than the first one in the presence of large velocity contrasts or to inaccuracies in the initial model. However, wave-equation traveltime inversion provides lower model resolution compared to conventional full waveform inversion. near-surface low velocity layer and resulting shingling data lead to inaccurate velocity estimates using ray-based methods. The workflow adopted in this paper tries to compensate for these issues by adding an intermediate wave-equation traveltime inversion to the conventional workflow.

SYNTHETIC DATA APPLICATION

To evaluate the performance of the new workflow, a synthetic dataset was constructed where the true velocity model has two low velocity layers with a background velocity that smoothly increases with depth. The starting model used in the inversion is the background velocity without the two low velocity layers. The velocity is laterally invariant. The maximum offset of the survey is 8 km. The synthetic data are

generated using constant density acoustic modeling engine. A typical shot gather (Figure 3) shows shingling as we move further away from source location. In the inversion, the source wavelet was known. We employed the workflow described above and ran the inversion using data with a peak frequency of 10 Hz. Inversion results are shown in Figure 4. The blue and red curves denote the true velocity model and the starting velocity model respectively, and the fuchsia curve is the inversion result. Notice that we were able to successfully recover both low velocity layers even when using relatively high frequencies. We also tried direct waveform inversion without wave-equation traveltime inversion using the same data. In this case, convergence to the right solution occurred only with peak frequencies of 7 Hz or lower.

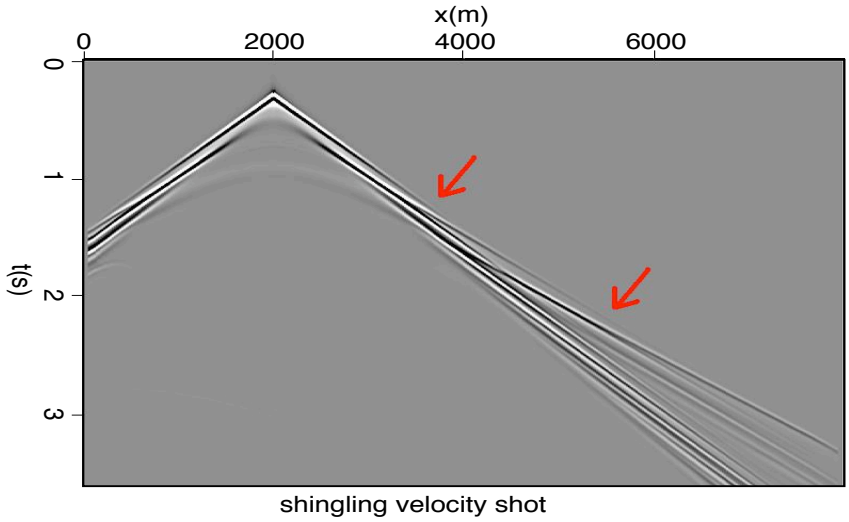

Figure 3: Synthetic shot gather by acoustic modeling using true velocity model. [**NR**]

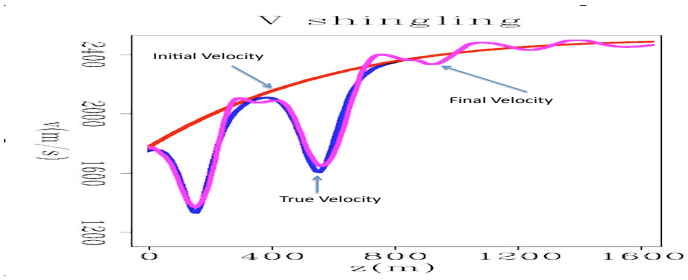

Figure 4: Inversion result with blue being true model, red being starting model and fuchsia being inverted model. [**NR**]

FIELD DATA APPLICATION

Our new workflow was applied to a 2D land dataset acquired in Saudi Arabia. The line geometry and the stacked section of the 2D data are shown in Figure 5. The

section of the line used for waveform inversion is between the two vertical red lines. The acquisition geometry was not strictly 2D, that is it was not in a straight line. The waveform inversion algorithm that was used is a 2D implementation of the time-domain approach described in Shen (2010). The line geometry was hence converted to 2D by a simple projection of the line onto the x-axis. The starting model was obtained by ray-based method using picked first-break traveltimes. Starting source wavelets were obtained by stacking part of the moved-out refractions, and vary from shot to shot. The source wavelets were then updated at each iteration of the inversion. We used a total of 110 shots, with 180m shot spacing and 30 m receiver spacing. Offset used for inversion ranged from -4000 to -400 m for each shot. The lowest frequency in the data was 10 Hz, which makes direct application of waveform-based inversion for the low frequencies of velocity difficult. Two waveform inversion runs were performed. The first run started directly from the first arrival traveltimes tomography model and the second run included an intermediate step of wave-equation traveltime inversion applied to the full bandwidth data.

The starting model and final results are shown in Figure 6. The inversion result after the wave-equation traveltime inversion shows a continuous low velocity event in the upper middle portion of the section

The reverse time migrated (RTM) images in Figure 7 clearly show that wave-equation traveltime inversion has improved the final image. Indeed, with better velocities, we get more spatial coherence, particularly in the neighborhood of the low velocity layer where reflections are seen both in the RTM result and on the stacked section in Figure 5 (indicated by the red ellipse).

Figure 8 shows ray tracing through the final velocity model within the data offsets used for inversion. This display verifies the depth of the valid velocity model updates, which in this case confirmed that the low velocity layer is indeed the result of inversion rather than an artifact. Since we are matching waveforms, it is also important to compare the modeled data with the input refraction data (Figure 9). It can be seen that waveforms and traveltimes match quite well despite differences in absolute amplitude. However, these difference are not a problem for the waveform-based waveform inversion objective function proposed by Shen (2010). Based on these results, the wave-equation traveltime inversion step seems to considerably improve the final results. This improvement could also be explained by the fact that the ray-based model was not totally consistent with the waveform inversion algorithm used.

CONCLUSION

We showed a new three stage waveform inversion workflow for near-surface velocity estimation:

```
1) First arrival traveltime tomography.
2) Wave-equation traveltime inversion.
```

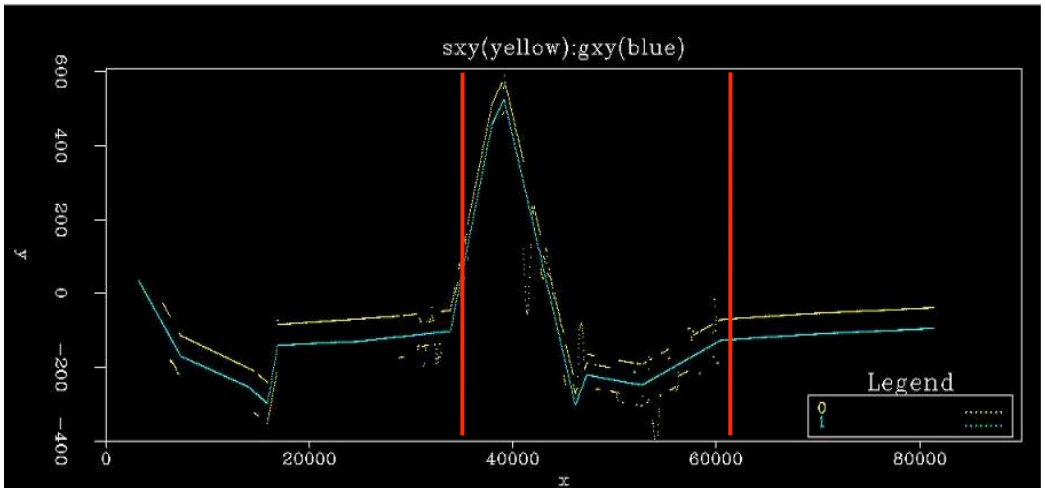

a)

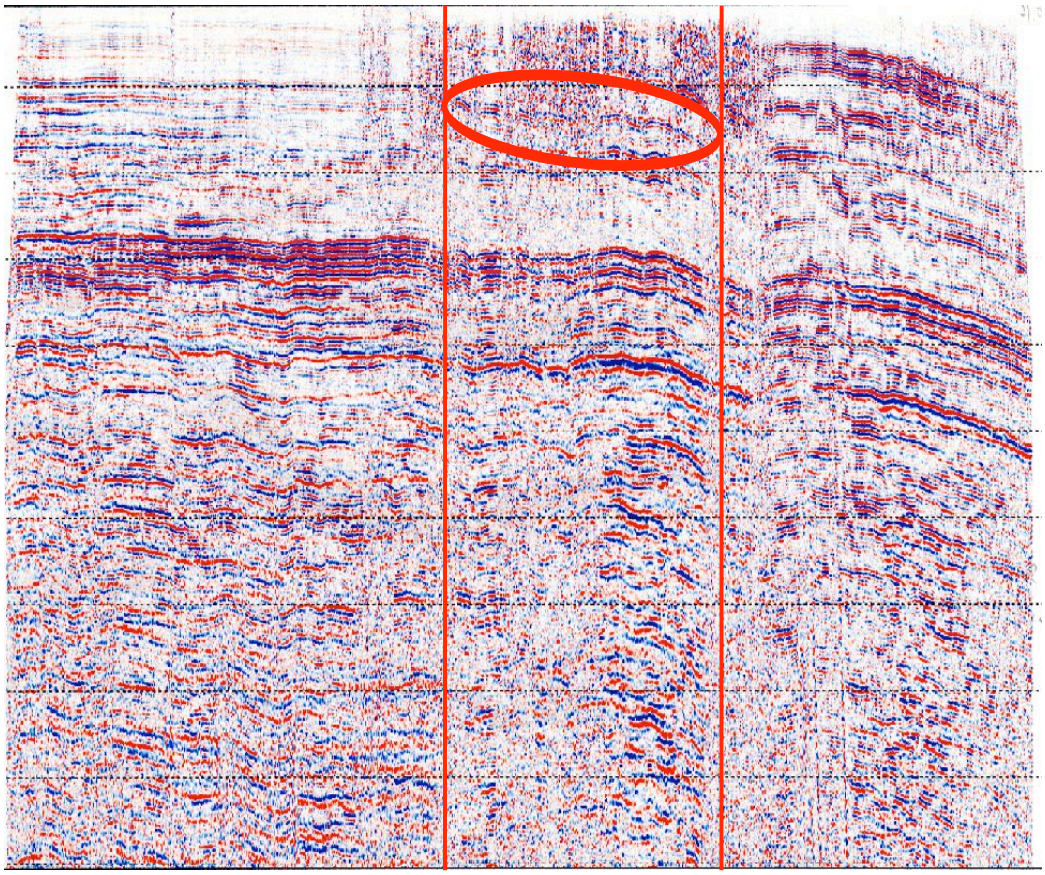

b)

Figure 5: A land 2D data case showing a) the x,y source receiver geometry, and b) the stacked. The area for waveform inversion is between the vertical red lines. Blue indicates source, and yellow indicates receiver locations. [**NR**]

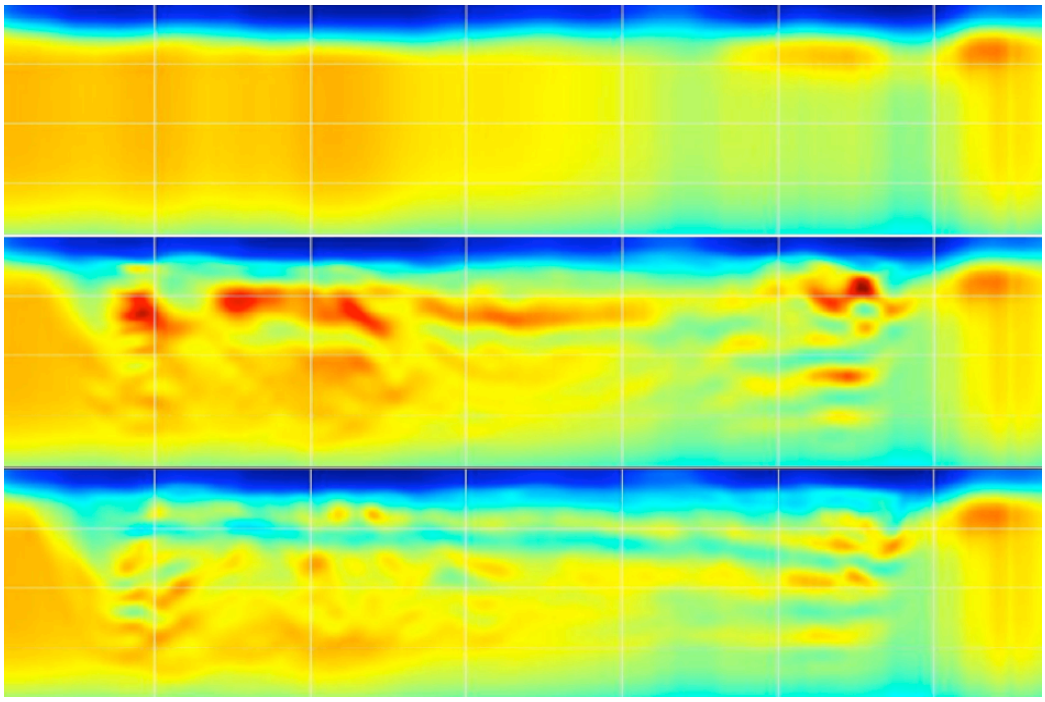

Figure 6: Starting depth velocity model using ray-based tomography (top), and waveform inversion results without (middle) and with (bottom) wave-equation traveltime inversion. [**NR**]

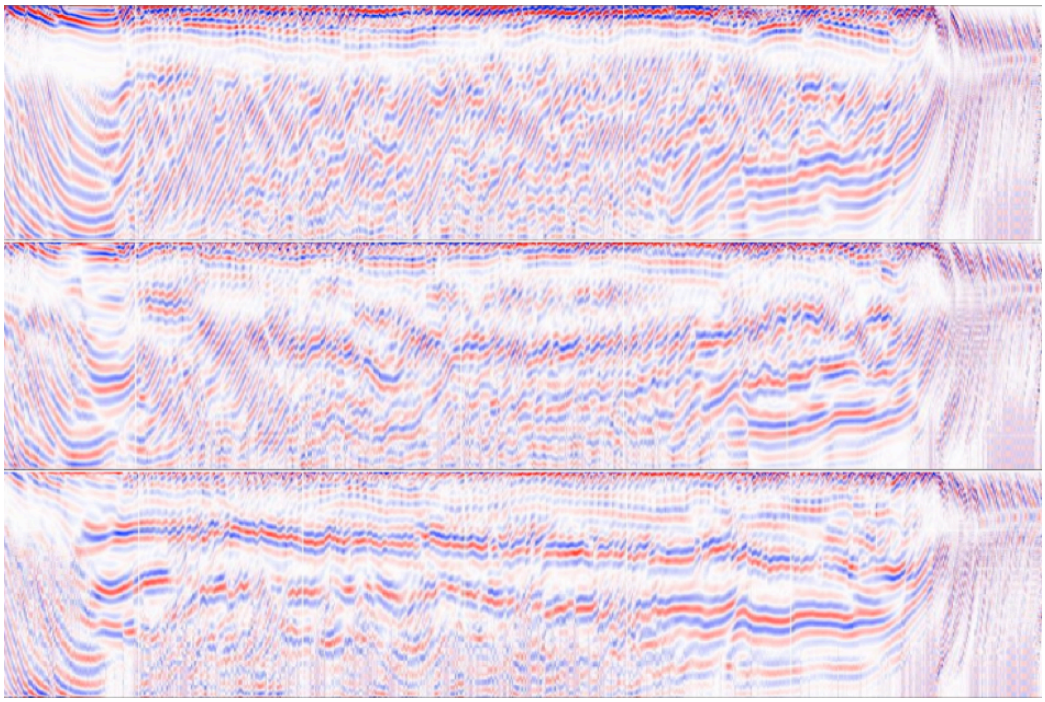

Figure 7: RTM images corresponding to the starting depth velocity model using ray-based tomography (top), and to the waveform inversion results without (middle) and with (bottom) wave-equation traveltime inversion. [**NR**]

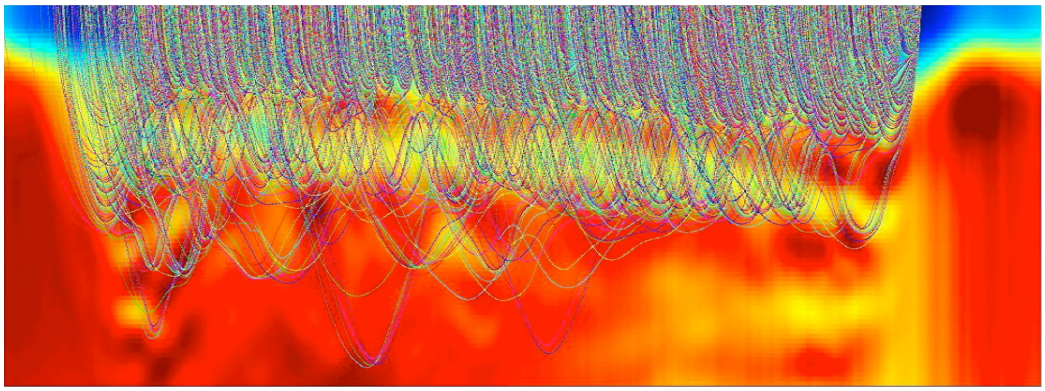

Figure 8: Ray tracing through the final velocity model. This shows that low velocity layer is indeed from inversion instead of being an artifact. [**NR**]

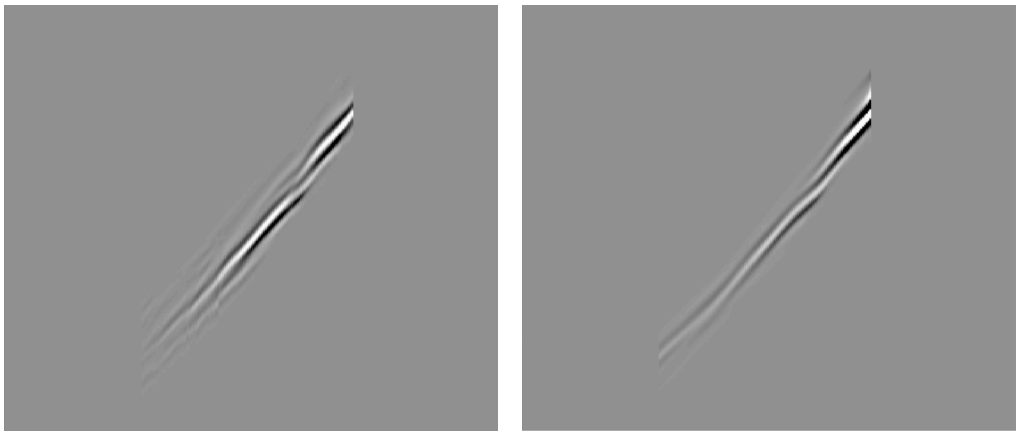

Figure 9: Comparison of a) input and b) modeled refractions. Note the similar kinematics despite minor differences in absolute amplitudes. [**NR**]

`3) Early arrival acoustic waveform inversion.`

The wave-equation traveltime inversion step helps correct inaccuracies in the conventional first arrival traveltime inversion result due to the inability of ray based methods to properly handle low velocity zones and large velocity contrasts.

This new workflow was evaluated using both a synthetic data example and a 2D field dataset from Saudi Arabia. Our new inversion workflow produced a superior result on the field data compared to results obtained using a more conventional strategy that did not include the wave-equation traveltime inversion step. Since the 2D field data was not acquired in a straight line, it is possible that the improvement we observed when using wave-equation traveltime inversion was partly due to the correction of the non-2D geometry. We plan to further investigate the wave-equation traveltime inversion, using a full 3D parametrization for the modeling and inversion.

ACKNOWLEDGMENTS

Xukai would like to thank the Geophysical Technology Team of the EXPEC Advanced Research Center, Saudi Aramco for providing the data and the financial support for this research. We would like to thank Saudi Aramco for allowing us to publish the result.

REFERENCES

Bevc, D., 1995, Imaging under rugged topography and complex velocity structure: SEP Ph.D Thesis.

Hampson, D. and B. Russell, 1984, First-break interpretation using generalized linear inversion: Journal of CSEG, **20**, 40–54.

Hindriks, C. and D. Verschuur, 2001, Common focus point approach to complex near surface effects: SEG Expanded Abstracts.

Luo, Y. and G. T. Schuster, 1991, Wave-equation traveltime inversion: Geophysics, **56**, 645–653.

Marsden, D., 1993, Statics corrections-a review: The Leading Edge.

Mora, P., 1987, Elastic wavefield inversion: SEP Ph.D Thesis.

Olson, K. B., 1984, A stable and flexible procedure for the inverse modelling of seismic first arrivals: Geophysical Prospecting, **37**, 455–465.

Pratt, R. G., C. Shin, and G. Hicks, 1998, Gauss-Newton and full Newton methods in frequency domain seismic waveform inversion: Geophysical Journal International, **133**, 341–362.

Ravaut, C., S. Operto, L. Improta, J. Virieux, A. Herrero, and P. Dell'Aversana, 2004, Multiscale imaging of complex structures from multifold wide-aperture seismic data by frequency-domain full-waveform tomography: application to a thrust belt: Geophysical Journal International, **159**, 1032–1056.

Shen, X., 2010, Near-surface velocity estimation by weighted early-arrival waveform inversion: SEG Expanded Abstracts.

Sheng, J., A. Leeds, M. Buddensiek, and G. T. Schuster, 2006, Early arrival waveform tomography on near-surface refraction data: Geophysics, **71**, U47–U57.

Sirgue, L., O.I.Barkved, J. V. Gestel, O. Askim, and R. Kommedal, 2009, 3d waveform inversion on valhall wide-azimuth obc: EAGE 71th Conference.

Tarantola, A., 1984, Inversion of seismic reflection data in the acoustic approximation: Geophysics, **49**, 1259–1266.

White, D. J., 1989, Two-dimensional seismic refraction tomogaphy: Geophysical Journal International, **97**, 223–245.


Arghh! This Makefile is really complicated!
That's what happens when you go elastic.
Yeah... and this is only 2D modeling
Just be careful.....
There is a Y axis coming.
OHAD